Short Papers

Modified Concentric Loop for Focused Electromagnetic Heating of Limbs and Torsos

Khalid A. Nabulsi and James R. Wait

Abstract—**An idealized two dimensional model of modified concentric loop for focused electromagnetic heating of limbs and torsos is considered. In contrast to the uniform current excitation, the present scheme has two current nulls diametrically opposite to one another. In this case, the circumferential electric field does not vanish on the axis which overcomes the principal criticism of the uniform loop.**

I. Introduction

The electromagnetic heating of limbs and torsos by induction has been a useful adjunct in cancer therapy. The simplest and most convenient scheme is a concentric wire loop excited by high or very high frequency current [1]. Many closely related schemes are discussed in a Special Issue of IEEE TRANSACTIONS ON MICROWAVE THEORY AND TECHNIQUES [2]. The main disadvantage of the closed loop with uniform current excitation is that the circumferential induced electric field E_ϕ within the idealized cylindrical conductor vanishes on the axis of the cylinder. On the other hand, most of the phased array schemes tend to excite an axial electrical field which is nonzero on the axis and may indeed have a local maximum [3]. Thus, from the standpoint of producing usable power along the axis, it would seem that axial electric field polarization is to be preferred. In fact, in this context, Rappaport [4] asserts that "the E_ϕ polarization is absolutely wrong." It is the purpose of this paper to propose a modified concentric loop which does not have the drawback of vanishing power deposition at the center of the cylinder.

The scheme we suggest is a circular loop with insulated breaks at opposite sides. Each of these semi-circular arcs is fed in phase such that the penetrated electric field has a maximum on the axis of the cylinder. In order to present the properties of the scheme, we shall present a brief analysis of a 2-D model which exhibits its salient properties.

II. Formulation

The geometry of the cylindrical target whose conductivity is σ mho/m and whose radius is a meters and which extends to infinity in the z-direction is shown in cross-section in Fig. 1. In cylindrical coordinates (r, ϕ, z), the cylinder is defined by $r = a$. The external region $r > a$ has a conductivity of σ_o mho/m, and the permeability is μ_o, the free space value, everywhere. At $r = b$ meters, we specify the source current density as $J_\phi(\phi)$ A/m which is assumed in this 2-D model to be constant for $-\infty < z < \infty$. In other words, the structure is to be excited by a cylindrical shell of current flowing only in the circumferential direction.

For the model as described, the magnetic field will have only an axial component H_z because the problem is independent of z. For a time factor $\exp(j\omega t)$, H_z satisfies a homogeneous Helmholtz equation everywhere except at $r = b$. The region $0 \le r < a$ is designated by region 1, the region $a < r < b$ is designated by region 2, and the region $r > b$ is designated by region 3. Thus, in the respective regions, H_z satisfies

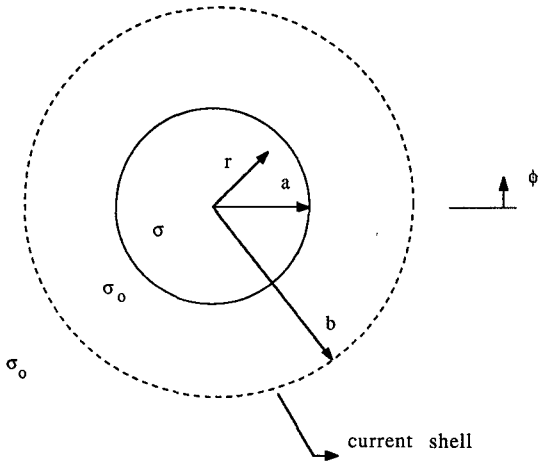

Fig. 1. The geometry of the model.

$$(\nabla^2_{r\phi} - \gamma^2)H_{z1} = 0 \qquad \text{for } 0 \le r < a \tag{1}$$

$$(\nabla^2_{r\phi} - \gamma_o^2)H_{z2} = 0 \qquad \text{for } a < r < b \tag{2}$$

$$(\nabla^2_{r\phi} - \gamma_o^2)H_{z3} = 0 \qquad \text{for } r > b \tag{3}$$

where

$$\nabla^2_{r_\phi} = \frac{1}{r}\frac{\partial}{\partial r}\left(r\frac{\partial}{\partial r}\right) + \frac{1}{r^2}\frac{\partial^2}{\partial \phi^2} \tag{4}$$

$$\gamma^2 = j\omega\mu_o\sigma \tag{5}$$

$$\gamma_o^2 = j\omega\mu_o\sigma_o. \tag{6}$$

Here, σ and σ_o can be regarded as complex to allow for the presence of displacement currents (e.g., replace σ by $(g + j\epsilon\omega)$ where g is the real conductivity and ϵ is the real permittivity of the target while σ_o can be replaced by $j\epsilon_o\omega$ if the external region is free space). In a practical scheme, not discussed here, the external region could be a bolus of conducting fluid.

From Maxwell's equations, the corresponding nonzero electric field components are obtained, for $r < a$, from

$$\sigma E_r = \frac{1}{r}\frac{\partial H_z}{\partial \phi} \tag{7}$$

and

$$\sigma E_\phi = -\frac{\partial H_z}{\partial r} \tag{8}$$

and the same equations hold for $r > a$ if σ is replaced by σ_o. The source condition is simply

$$\lim_{\Delta \to 0}\left[H_{z2}(r = b - \Delta) - H_{z3}(r = b + \Delta)\right] = J_\phi(\phi). \tag{9}$$

Manuscript received September 17, 1991; revised January 7, 1992.

The authors are with the Department of Electrical and Computer Engineering, University of Arizona, Tucson, Arizona 85721.

IEEE Log Number 9107022.

The appropriate Fourier series representation for the source current density is

$$J_\phi(\phi) = \sum_m J_m \cos m\phi \tag{10}$$

where the summation here, and in what follows, is over only the odd positive values of m (i.e., $m = 1, 3, 5, \cdots$). Once the $J_\phi(\phi)$ is specified, the coefficient J_m is obtained from

$$J_m' = \frac{4}{\pi}\int_0^{\pi/2} J_\phi(\phi) \cos m\phi \, d\phi. \tag{11}$$

The desired solutions satisfying (1), (2), and (3) have the forms

$$H_{z1} = \sum_m A_m I_m(\gamma r) \cos m\phi \qquad (0 < r < a) \tag{12}$$

$$H_{z2} = \sum_m [B_m I_m(\gamma_o r) + C_m K_m(\gamma_o r)] \cos m\phi \qquad (a < r < b) \tag{13}$$

$$H_{z3} = \sum_m D_m K_m(\gamma_o r) \qquad (r > b) \tag{14}$$

where I_m and K_m are modified Bessel functions of order m and of the indicated arguments and where A_m, B_m, C_m, and D_m are coefficients to be determined.

The boundary conditions at $r = a$ are that E_ϕ and H_z be continuous. Also, the source condition (9) is augmented by the required continuity of E_ϕ at $r = b$. Thus the four coefficients are expressible in terms of J_m. For the present purposes, we will just state the result for the first coefficient A_m, or

$$A_m = J_m(b/a)K_m'(\gamma_o b)[I_m(\gamma_a)K_m'(\gamma_o a) - (\eta/\eta_o)I_m'(\gamma a)K_m(\gamma_o a)]^{-1} \tag{15}$$

where $\eta = j\mu_o\omega/\gamma = (j\mu_o\omega/\sigma)^{1/2}$ and $\eta_o = j\mu_o\omega/\gamma_o = (j\mu_o\omega/\sigma_o)^{1/2}$ are intrinsic wave impedances. The primes indicate differentiation of the modified Bessel's functions with respect to the indicated arguments.

The radial and azimuth electric fields inside the cylinder ($r < a$) are of special interest. They are obtained from (7) and (8) and are given explicitly by

$$E_r = \frac{-1}{\sigma r}\sum_m mA_m I_m(\gamma r) \sin m\phi \tag{16}$$

and

$$E_\phi = -\frac{\gamma}{\sigma}\sum_m A_m I_m'(\gamma r) \cos m\phi \tag{17}$$

the power dissipated at any interior point is obtained from

$$P = \tfrac{1}{2}\,\mathrm{Re}\,(\sigma)(|E_r|^2 + |E_\phi|^2) \qquad \text{in watts}/m^3. \tag{18}$$

Of special interest is the value of P on the axis. In this case, we observe that, in the limit as $r \to 0$, both $(\gamma r)^{-1} I_m(\gamma r)$ and $I_m'(\gamma r)$ tend to $\frac{1}{2}$ for $m = 1$, but zero otherwise. Then, it is a simple matter to deduce that the power dissipation P_o on the axis is given by

$$P_o = \lim_{r\to 0} P = \tfrac{1}{8}|A_1|^2\,\mathrm{Re}\,(\sigma)|\gamma|^2/|\sigma|^2 \qquad \text{watts}/m^3. \tag{19}$$

It is interesting to observe here that the higher harmonics (i.e., $m = 3, 5, 7, \cdots$) play no role in providing power on the axis. Thus, it might be concluded that the optimum excitation in this context would be to set $J_m = 0$ except for $m = 1$. The corresponding current excitation in that case would be $J_\phi(\phi) = J_1 \cos\phi$. For this situation the power $P(r, \phi)$ deposition within the cylinder (i.e., for $0 \le r < a$) would be given by

$$P(r, \phi) = \tfrac{1}{2}[\mathrm{Re}\,(\sigma)/|\sigma|^2][r^{-2}|I_1(\gamma r)|^2 \sin^2\phi + |\gamma|^2|I_1'(\gamma r)|^2\cos^2\phi]\,|A_1|^2. \tag{20}$$

This function of r and ϕ could be employed to map relative power deposition over the cross-section of the cylinder without having to evaluate A_1 which does not depend on r and ϕ. For example, if we just look at the variation over the central plane $\phi = \pm\pi/2$, we would have

$$P(r, \pi/2) = 4P_o[|\gamma r|^{-2}|I_1(\gamma r)|^2]. \tag{21}$$

On the other hand, if we examine the power deposition over the transverse plane $\phi = 0, \pi$;

$$P(r, 0) = 4P_o[|I_1'(\gamma r)|^2]. \tag{22}$$

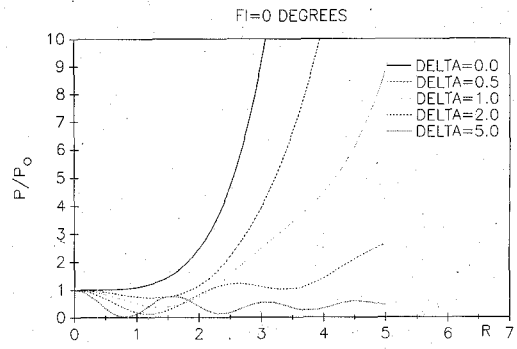

Fig. 2. Power focusing relative to power at the center versus R for $\phi = 0$ degrees.

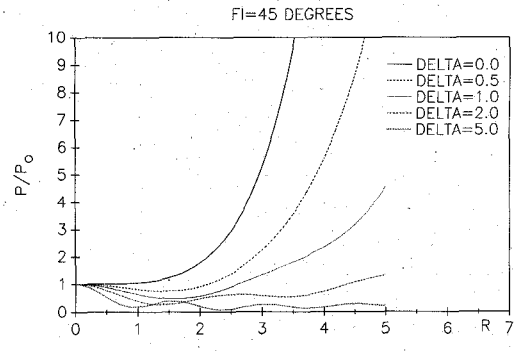

Fig. 3. Power focusing relative to power at the center versus R for $\phi = 45$ degrees.

III. Numerical Results

For plotting, we write γr as

$$\gamma r = e^{j\pi/4}R(1 + j\Delta)^{1/2} \tag{23}$$

where

$$R = \sqrt{\mu_o\omega g}\,r \tag{24}$$

$$\Delta = \epsilon\omega/g \tag{25}$$

and g is the real conductivity. The function $P(R, \phi)/P_o$ is plotted in Figs. 2, 3, and 4 *versus* R from 0 to $R_a = 5$ where R_a is obtained from (24) with r replaced by a, and for $\Delta = 0$, 0.5, 1.0, 2, and 5. Fig. 2 is for $\phi = 0°$, Fig. 3 is for $\phi = 45°$, and Fig. 4 is for $\phi = 90°$. $R = 0$ corresponds to the center of the cylinder. It is clear that as Δ increases (i.e., as frequency increases), the power be-

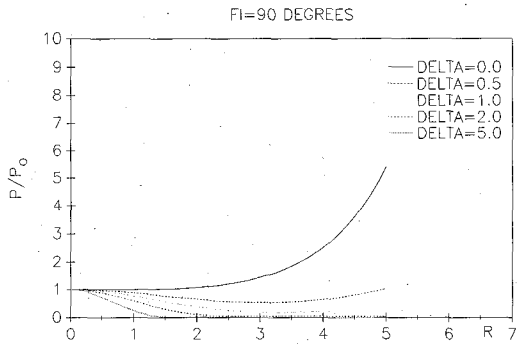

Fig. 4. Power focusing relative to power at the center versus R for ϕ = 90 degrees.

comes focused near the center of the cylinder. At low frequency (i.e., Δ is small where displacement current is negligible) there is no focusing.

IV. Concluding Remarks

While the present model is highly idealized, it does show that, with a cos ϕ excitation, the power can be focused on the axis of the cylinder. To deal with a cylinder of finite length and an actual wire loop, a three-dimensional analysis is required, but we can assert that in the principal plane of the loop, the result should be qualitatively similar to the two-dimensional model. Of course, for a practical scheme, we would limit the cylinder radius a to reduce the peripheral heating.

References

[1] F. K. Storm, R. S. Elliott, W. H. Harrison, and D. L Morton, "Clinical RF hyperthermia by magnetic loop induction: A new approach to human cancer therapy," *IEEE Trans. Microwave Theory Tech.*, vol. 30, no. 8, pp. 1149–1157, Aug. 1982.

[2] J. C. Lin, Ed., Special Issue on Phased Arrays, *IEEE Trans Microwave Theory Tech.*, vol. 34, no. 5, pp. 481–648, May 1986.

[3] J. R. Wait and M. Lumori, "Focused heating in cylindrical targets," Pt. II., *IEEE Trans.*, vol. 34, no. 3, pp. 357–359, Mar. 1986.

[4] C. M. Rappaport, "Synthesis of optimum microwave antenna applications for use in treating deep localized tumors," in *Progress in Electromagnetic Research*. Amsterdam: Elsevier, vol. 1, no. 2, 1989, pp. 175–240.

Bias-Dependence of the Intrinsic Element Values of InGaAs/InAlAs/InP Inverted Heterojunction Bipolar Transistor

Bahman Meskoob, Sheila Prasad, Mankuan Vai, James C. Vlcek, Hiroya Sato, and Clifton G. Fonstad

***Abstract*—The small-signal S parameters of an inverted InGaAs/InAlAs/InP heterojunction bipolar transistor are measured at 39 bias points covering the entire useful bias region. Small-signal model fitting is performed at each bias point. The results of the small-signal model fitting show that in this device it is sufficient to take five intrinsic elements of the model to be bias dependent. The methodology and the results of the simulations are presented here.**

Manuscript received July 30, 1991; revised November 15, 1991. This work was supported in part by NSF grant ECS-9005837 to Northeastern University.

B. Meskoob, S. Prasad, M-K. Vai are with the Department of Electrical and Computer Engineering, Northeastern University, Boston, MA, 02115.

C. F. Fonstad is and J. C. Vlcek was with the Department of Electrical Engineering and Computer Science and Center for Materials Science and Engineering, Massachusetts Institute of Technology, Cambridge, MA 02139. J. C. Vlcek is now with Epi Corporation, St. Paul, MN 55101.

H. Sato is with the Sharp Corporation, Nara 632, Japan.

IEEE Log Number 9107023.

I. Introduction

The heterojunction bipolar transistor (HBT) is rapidly emerging as a significant device for applications at microwave frequencies. Kim *et al.* [1] have reviewed the GaAs device and IC technology in detail. There has also been a rapid development of the InP/In(Al, Ga)As HBT technology [2] and the inverted HBT structure is being explored [3]. A small signal equivalent circuit model has been developed [4] for this structure. However, for many microwave applications, it is also necessary to have a large-signal model.

For large signal device modeling, the voltage and/or current dependence of the model elements is required. The dynamic variation of the element values has usually been assumed to be the same as the static (or bias) variation. This assumption has been proved to work quite well for many design applications. The popularity of this *quasi-static* assumption is due to the simplicity of small signal measurements and the subsequent modeling of transistors.

As a first step towards the large signal modeling, we have investigated the bias dependence of five intrinsic elements of the small signal model of the inverted HBT having the layer structure shown in Fig. 1. This has been done through small-signal S parameter measurements and model fitting using the commercial software Touchstone [5]. The results are presented in this paper.

II. Procedure

Fig. 2 shows the HBT's I-V characteristics. Small-signal S parameters were measured on wafer from 0.05 to 40 GHz at 39 different bias points. These were chosen along constant base current (I_b) curves at different V_{ce} values. Since this device has an f_T of 23 GHz, measurements above 26 GHz were not used for modeling. To reduce the computation time, only 16 frequencies were chosen. These are 0.05, 0.1, 0.2, 0.4, 0.8, 1.6 GHz; 3 to 11 GHz in 2 GHz increments and 11 to 26 GHz in 3 GHz increments.

The small signal equivalent circuit is shown in Fig. 3. Initially this model was fitted to measurements at the bias point of I_b = 150 μA, V_{ce} = 1.6 V. Due to the large number of parameters (element values) in the optimization process, it is difficult to judge the physical validity of the optimized parameters. In order to test the validity of the element values, a fit at zero bias (I_b = 0 μA, V_{ce} = 0 V) was performed. Since at zero bias the device is passive (α_o = 0) and both R_e and R_o (= $1/g_o$) are very large, three of the five bias-dependent elements are effectively removed. Therefore, a variation of only two bias-dependent elements (namely, C_e and C_c) should result in a good fit at zero bias. The fit at (150 μA, 1.6 V) was modified until the zero bias fit was also acceptable. Fig. 4 shows the normalized deviation defined by

$$\text{Normalized Deviation} = \frac{1}{39}\sum_{\text{Bias}}\left|\frac{M-S}{M}\right|$$

where M is the measured and S is the simulated vector S parameter and the number of bias points used is 39. The deviation is typically within 10% except for S_{12} at low frequencies. Due to the small magnitude of S_{12} at low frequencies, any error in its measured magnitude or phase results in a significant error in the calculation of the normalized deviation.